

# Final Report for Summer Internship 2020

## Part II: Experiments with Qiskit Open-Pulse

Harshvardhan K. Babla

*Advised By:* Tudor-Alexandru Petrescu, Alexandre Blais

November 26, 2020

### Contents

<b>1</b>	<b>Introduction</b>	<b>2</b>
<b>2</b>	<b>System Calibration</b>	<b>2</b>
<b>3</b>	<b>Cavity Sweep to Derive <math>\chi</math></b>	<b>2</b>
<b>4</b>	<b>Single Shot Readout in the IQ Plane</b>	<b>5</b>
4.1	Varying Readout Power . . . . .	5
4.2	Varying Delay Time (Population Dynamics) . . . . .	9
4.3	Population Dynamics for Various Powers . . . . .	10
4.4	Abnormalities with the measurement . . . . .	11
<b>5</b>	<b><math>T_1</math> vs Measurement Amplitude</b>	<b>14</b>
<b>6</b>	<b>Discussion on the Limitations of Open-Pulse and Unsuccessful Experiments</b>	<b>15</b>

# 1 Introduction

The goal of this project was to characterize the trend between the qubit's  $T_1$  and the cavity population,  $\bar{n}$ . This document summarizes the experiments I ran on the IBM Quantum Experience (through Qiskit Open-Pulse).

Please refer to Part I, for a discussion on the theory I learnt this summer and experimental analysis of data collected by the HouckLab.

## 2 System Calibration

The qiskit textbook <sup>1</sup> has an extensive explanation on how to calibrate the devices. I essentially reran their code (with very little changes) before every experiment, to calibrate the qubit frequency, calibrating the  $\pi$ -pulse, and measuring  $T_1$ .

## 3 Cavity Sweep to Derive $\chi$

To look for the device's cavity pull,  $\chi$  we sweep the measurement frequency around the cavity frequency when the qubit is initialized in the ground and excited states. Theory (explained in Part I) predicts the cavity response to be a lorentzian in magnitude and an arctan in phase. The resonant frequency of the cavity is expected to shift depending on the state of the qubit.

As shown in Fig. 3(a) and (b), a cavity sweep on the Armonk device reveals two well separated dips in the magnitude of the signal and phase shifts in phase. While the magnitude data doesn't fit well to a Lorentzian, the phase data clearly seems to be an arctan sitting on top of a linear function. We can fit the phase data to  $A \arctan(\omega_{meas} - \phi) + mx + b$ , and derive the plot in Fig. 3(c). Removing the linear term, we obtain the corrected phase data as in Fig. 3(d), which we can use to derive the cavity's  $\chi$ . However, this analysis isn't replicated too well for other devices on the IBMQ cloud. Fig. 3 shows the magnitude of the signal for cavity sweeps on different qubits in the Montreal and Almaden systems. These results show that the peaks of the cavity sweep aren't centered extremely close for a qubit initialized in the ground or excited state. This is seen in the Bogota system as well, as shown in Fig. 3(a). This motivates us to sweep a wider range of frequencies in Bogota. As shown in Fig. 3(b), the magnitude response seems to be closer to a  $|\text{sinc}(\omega)|$  function. This is seen in the phase plot as well, where we observe a  $\pi$  jump in phase whenever the response crosses zero.

To investigate the presence of a sinc function, we go back to the Cavity-Bloch equations.

$$\frac{d}{dt} \langle a \rangle_{g/e}(t) = -i\epsilon(t) - i(\Delta_c \pm \chi) \langle a \rangle_{g/e}(t) - \frac{\kappa}{2} \langle a \rangle_{g/e}(t)$$

In the Fourier domain,

$$i\omega \langle a \rangle_{g/e}(i\omega) = -i\epsilon(i\omega) - i(\Delta_c \pm \chi) \langle a \rangle_{g/e}(i\omega) - \frac{\kappa}{2} \langle a \rangle_{g/e}(i\omega)$$

For a constant drive,  $\epsilon(t) = \epsilon$ , we recover the Lorentzian.

$$\langle a \rangle_{g/e}(i\omega) = \delta(i\omega) \frac{-\epsilon}{\omega + (\Delta_c \pm \chi) - i\frac{\kappa}{2}}$$

---

<sup>1</sup><https://qiskit.org/textbook/ch-quantum-hardware/calibrating-qubits-pulse.html>

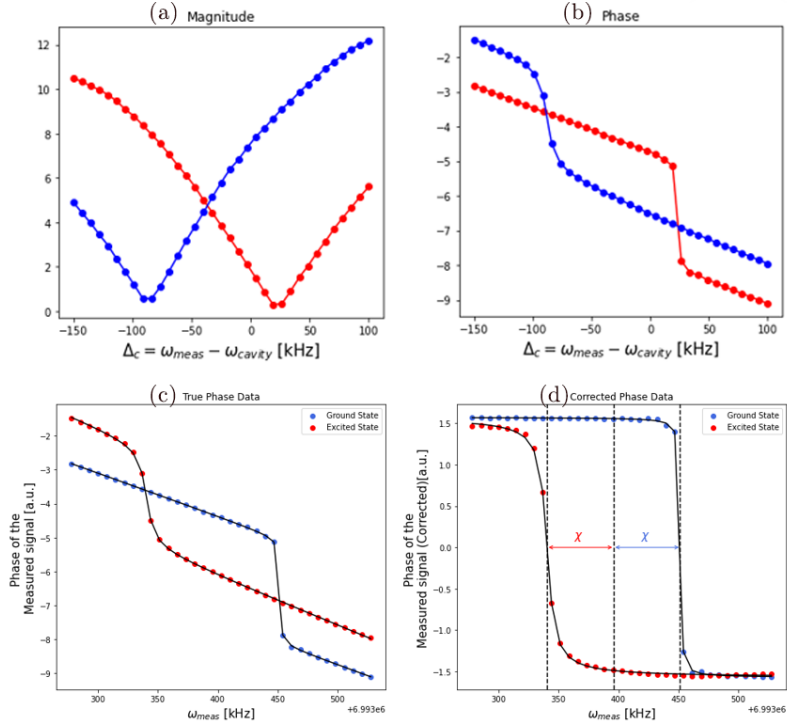
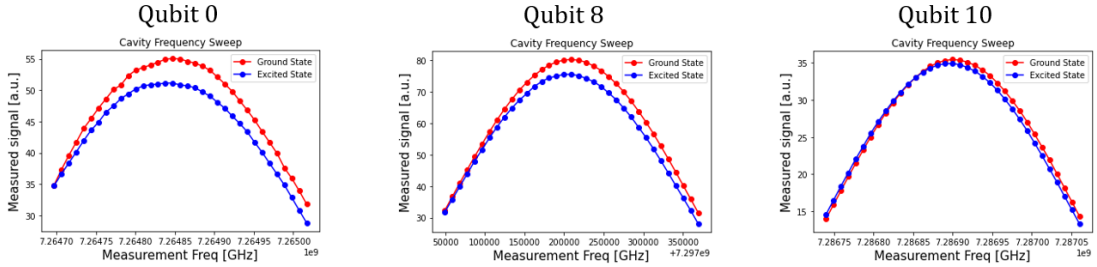


Figure 1: The magnitude (a) and phase (b) of the cavity frequency sweep for a qubit initialized in the ground (red) and excited (blue) state. Panel (c) shows the phase data fit to an arctan sitting on a linear function, whereas (d) corrects the data by removing the linear dependence.

## Almaden



## Montreal

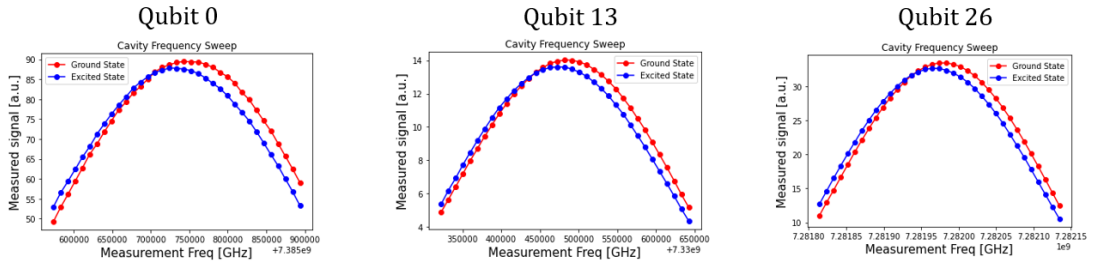


Figure 2: The magnitude of the cavity frequency sweep for a qubit initialized in the ground (red) and excited (blue) state.

However, for a box-forcing term:

$$\epsilon(t) = \epsilon \text{Box}_T(t) \rightarrow \epsilon(i\omega) = \epsilon \int_{-T/2}^{T/2} e^{-i\omega t} dt = \text{sinc}\left(\frac{T}{2}\right) \quad (1)$$

$$\langle a \rangle_{g/e}(i\omega) = \text{sinc}_T(i\omega) \frac{-\epsilon}{\omega + (\Delta_c \pm \chi) - i\frac{\kappa}{2}} \quad (2)$$

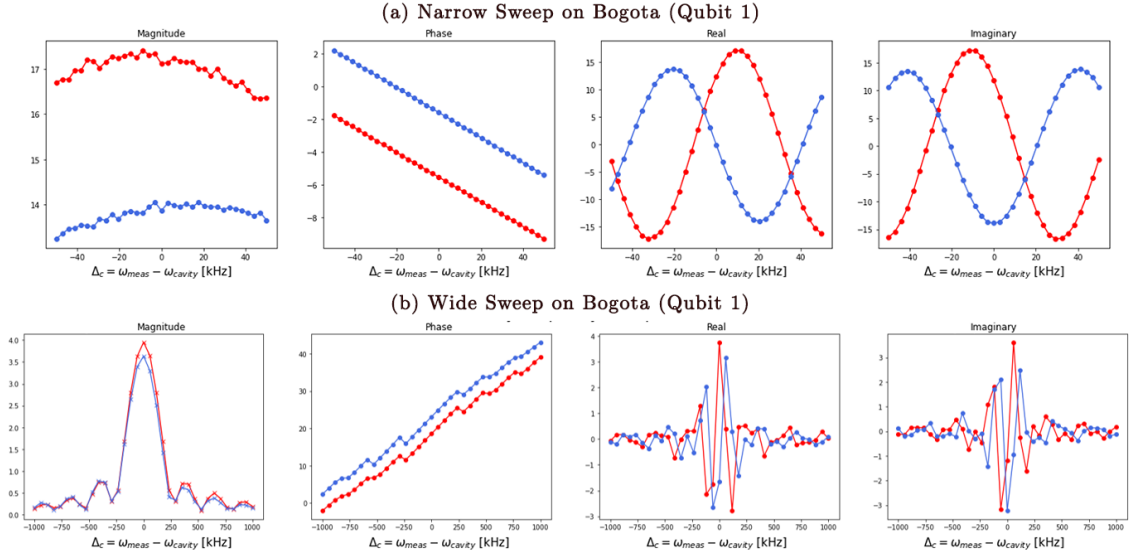


Figure 3: (a) Narrow and (b) wide cavity sweeps on Qubit 1 in the Bogota system. We show the magnitude, phase, real, and imaginary parts of the signal for a qubit initialized in the ground (red) and excited (blue) state.

Taking the inverse Fourier transform, we have

$$\langle a \rangle_{g/e}(t) = \int_{-\infty}^{+\infty} e^{+i\omega t} \text{sinc}_T(i\omega) \frac{-\epsilon}{\omega + (\Delta_c \pm \chi) - i\frac{\kappa}{2}} d\omega \quad (3)$$

According to this analysis, we expect the qubit response to be closer to a sinc, if we measure for a time much smaller than the time-scale  $2/\kappa$ . However, as we increase the measurement-time, the sinc function tends to a delta function and we recover the qubit Lorentzian peak.

Figure 3 shows the results of increasing the measurement time. As we increase the duration of the measurement tone, we see the sinc function become narrower. However, the width saturates quite quickly and we don't see any noticeable change for measurement pulses longer than  $4.0\mu s$ . After conversing with the IBM staff, we realize this issue exists as the backend truncates long pulses. In conclusion, we were unable to derive  $\chi$  on devices other than Armonk.

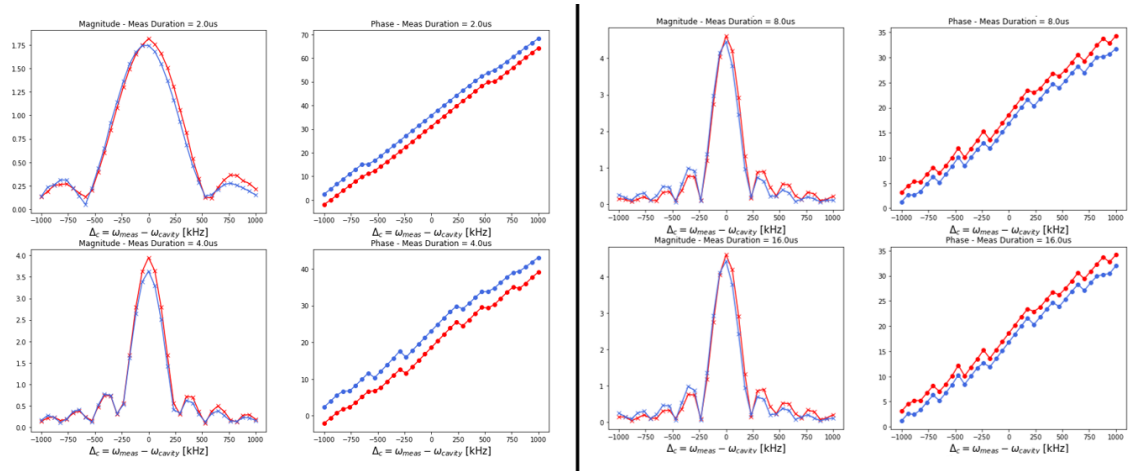


Figure 4: The cavity frequency sweep data (magnitude and phase) for the measurement duration equal to (a)  $2.0\mu s$ , (b)  $4.0\mu s$ , (c)  $8.0\mu s$ , and (d)  $16.0\mu s$ . For reference, the pulse calibrated by the backend is  $4.0\mu s$  long.

## 4 Single Shot Readout in the IQ Plane

### 4.1 Varying Readout Power

To investigate how the single shot IQ data changes with the readout power, we vary the amplitude of the measurement tone. Qiskit allows us to vary the measurement amplitude between the dimensionless limits 0 and 1. A selection of the IQ-plane measurements at various amplitudes is shown in Fig. 5.

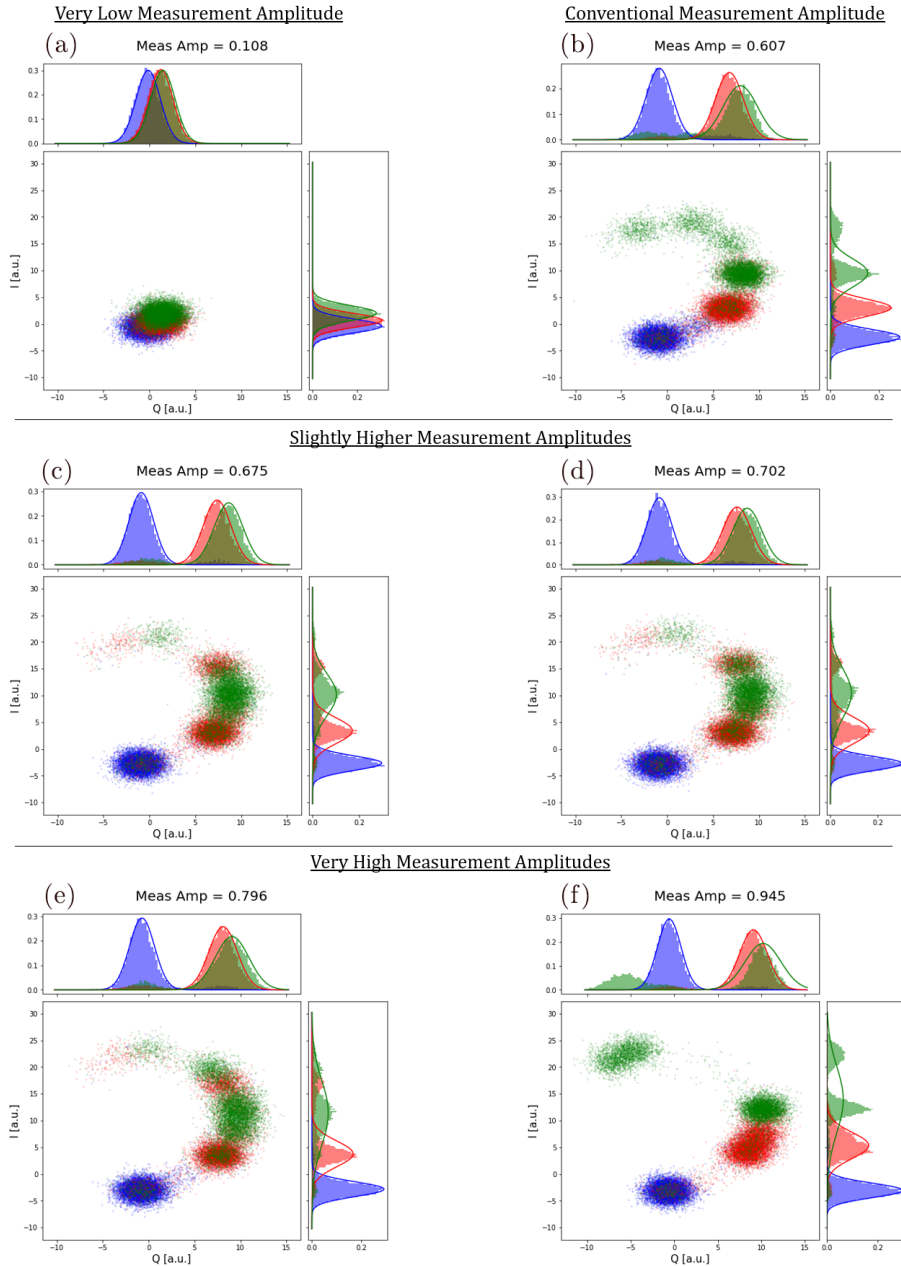


Figure 5: IQ measurements vs. amplitude of the measurement tone, for the ground (blue), excited (red), and f (green) states. The measurement amplitudes are (a) 0.108, (b) 0.607, (c) 0.675, (d) 0.702, (e) 0.796, and (f) 0.945. The density of the points in I and Q have been plotted on the side of the IQ plane, along with the respective Gaussian fits.

Observe that the coherent states corresponding to the respective states move apart as we in-

crease the measurement amplitude. However, at very high amplitudes the coherent states become distorted and sometimes split in two.

A single job sent to the IBMQ server included measurements of the  $|g\rangle$ ,  $|e\rangle$ , and  $|f\rangle$  states at 25 powers each (maximizing the 75 experiments per job limit). Five such jobs spanned different measurement amplitudes, creating the overall experiment that measures the single shot IQ data as a function of the readout power.

Fig. 6 shows the magnitude and phase of the cavity field, averaged over all the single shot measurements. We see that the magnitude of the cavity field (for all three states) consistently increases with the measurement amplitude, with a rate dependant on the qubit's state. This implies that the separation between the coherent states increases as we increase the amplitude of the measurement tone. On the other hand, the phase of the signal is relatively constant with respect to the measurement amplitude, as predicted by theory. The corresponding theory is found in Part I of the report.

Observe that fractures can be seen in both plots. Each segment corresponds to a collection of experiments within a single job. This suggests that the backend isn't consistent across jobs.

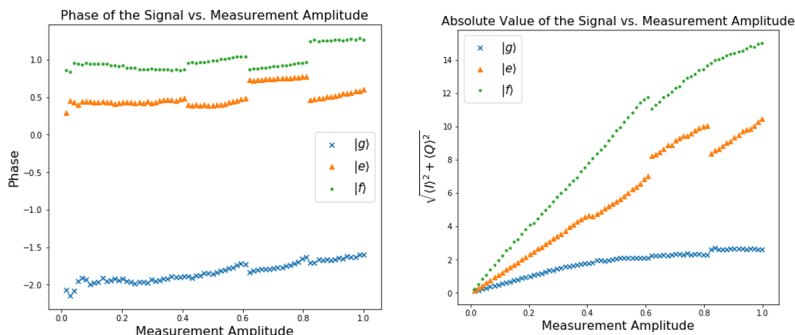


Figure 6: Magnitude and Phase of the cavity field (averaged over all the single shot measurements).

Signal is found in the separation of the Gaussians, whereas the error is found in the overlap between the Gaussians. Therefore, we define the SNR as given by Blais et. al. (2020).

$$\text{SNR} = \frac{|\mu_g - \mu_e|}{\sqrt{\sigma_g^2 + \sigma_e^2}}$$

Fig. 7 shows the SNR as a function of the power, which has been computed using the fitted Gaussians. We observe that the SNR is only high when the ground state is involved, this is expected as the  $|e\rangle$  and  $|f\rangle$  Gaussians in Fig. 5 are separated largely in I rather than Q.

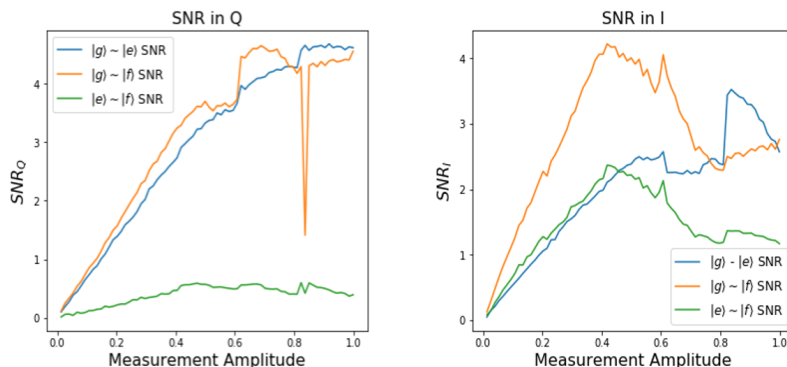


Figure 7: The SNR of the measurement for the I and Q quadratures as a function of the amplitude of the measurement tone. The plots are  $|g\rangle \sim |e\rangle$  SNR (blue),  $|g\rangle \sim |f\rangle$  SNR (orange), and  $|e\rangle \sim |f\rangle$  SNR (green) Gaussian fits.

SNR in the I-quadrature initially increases with the measurement amplitude but falls quickly for very high measurement amplitudes. This can be explained as we see not only the coherent states move apart with increasing the measurement amplitude, but also significant distortion at very high measurement amplitude. Secondly, at very high measurement amplitudes we see that the  $|e\rangle$  state blob overlaps significantly with the  $|f\rangle$  state blob.

Figure 8 shows the abnormal results from a measurement where just the  $|g\rangle$  and  $|e\rangle$  results were measured, whereas 9 shows the results from an experiment where all three states were measured.

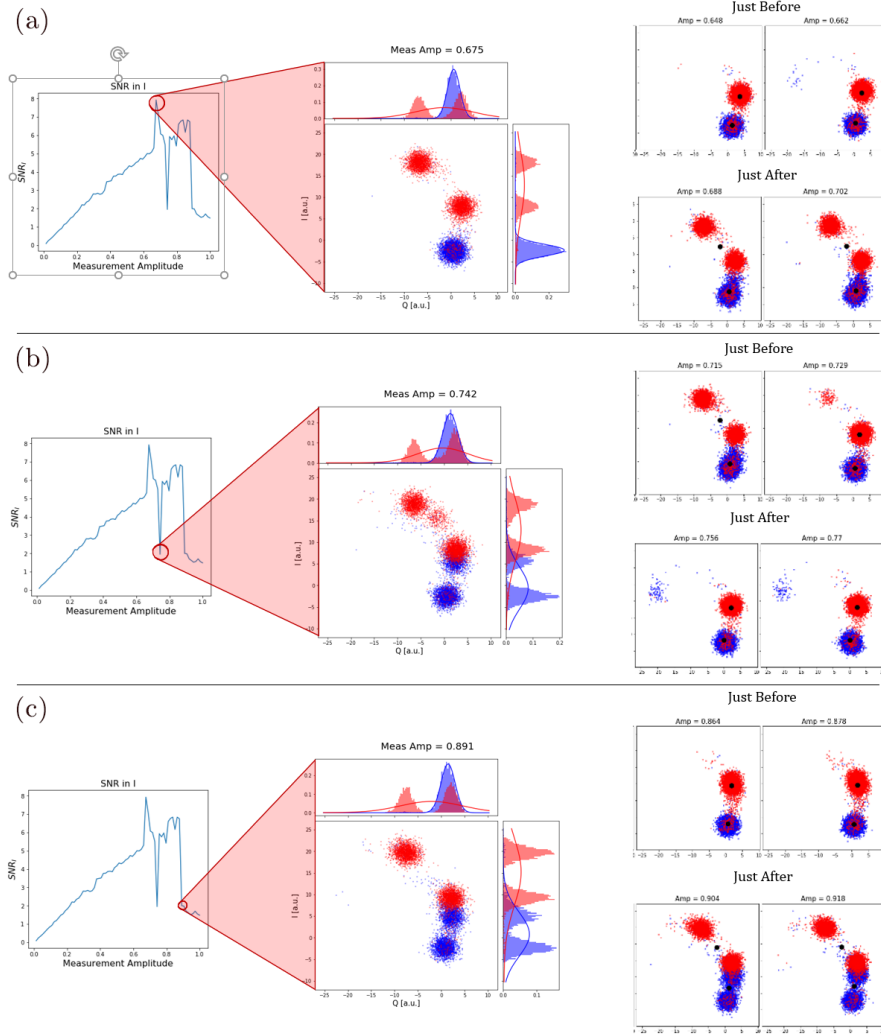


Figure 8: Abnormal IQ plots for particular set of measurement amplitudes. The measurement amplitudes are (a) 0.675, (b) 0.742, and (c) 0.891. These points are abnormal in the sense that they're distinctly different in the trend found in  $|g\rangle \sim |e\rangle$  SNR plot. The IQ plots for the measurement amplitudes just before and just after the abnormal point have also been plotted.

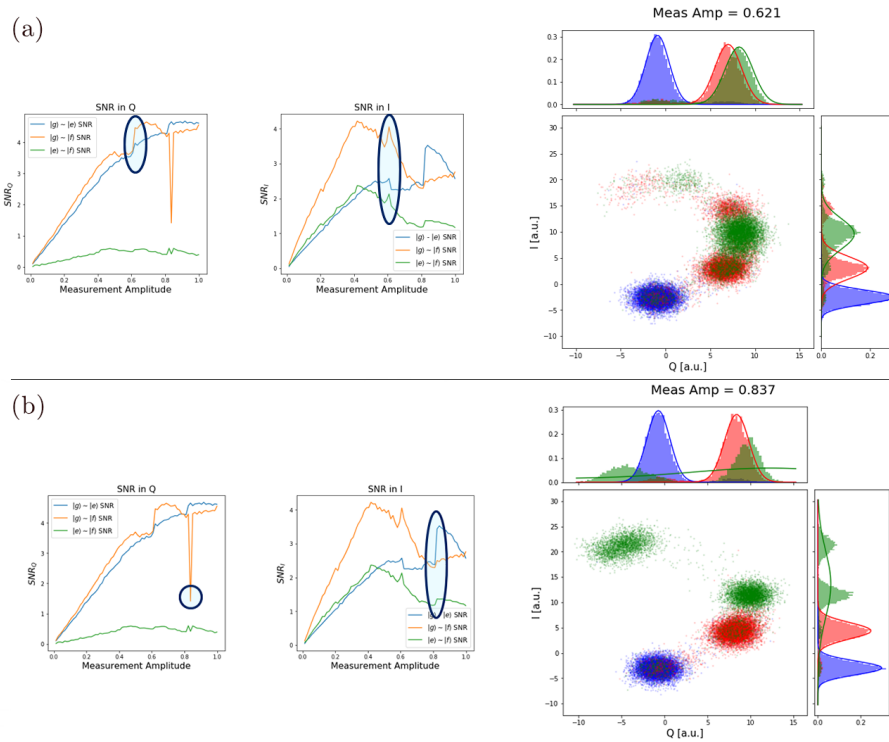


Figure 9: Abnormal IQ plots for particular set of measurement amplitudes (based on the experiment where  $|g\rangle$ ,  $|e\rangle$  and  $|f\rangle$  states were measured). The measurement amplitudes are (a) 0.621 and (b) 0.837.

## 4.2 Varying Delay Time (Population Dynamics)

We can also explore how the cavity field in the IQ plane evolves with time for the different states. Fig. 10(a) shows the coherent states corresponding to the  $|g\rangle$ ,  $|e\rangle$ , and  $|f\rangle$  states at different times, since they were initialized. Observe that the location of the blobs doesn't change. However, the number points in the  $|e\rangle$  and  $|f\rangle$  state blobs decreases with time. This implies that as the population decays, it becomes less and less likely for the qubit to be excited.

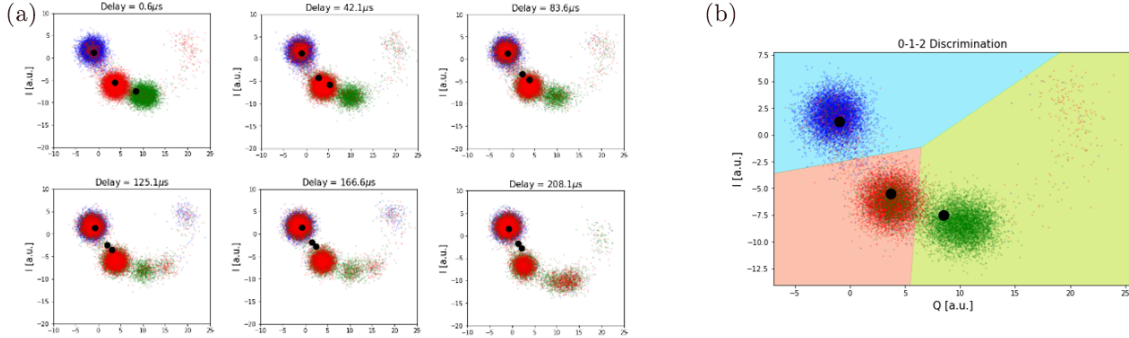


Figure 10: (a) Cavity field measured for the  $|g\rangle$ (blue),  $|e\rangle$ (red), and  $|f\rangle$ (green) states at various times since initialization. (b) Separation of the IQ plane into three using an LDA classifier. The data shown is at from the earliest time-stamp of  $0.6\mu s$  since initialization. In both panels, the big black dots represent the mean values of all the single shot measurements for the given state.

We can use this data to plot the average population dynamics of the coherent states. As shown in Fig. 10(b), we use Linear Discriminant Analysis (LDA) and the data from the earliest time-stamp at  $0.6\mu s$  to divide the IQ plane into subspaces corresponding to each of the three states. We can use this classifier to determine the number of points in each of the three subspaces, for a given coherent state. We call the fraction of points present in the subspace corresponding to state  $|x\rangle$ , the “population” in the  $|x\rangle$  state.

Fig. 11 shows the population dynamics as a function of time. Just as before, we see fractions in the curve at points where the job was split. When the qubit is initialized in the ground state,  $|g\rangle$  most of the population stays within  $|g\rangle$ . The population in  $|e\rangle$  and  $|f\rangle$  is non-zero, likely because of the spreading of the coherent state. When the qubit is initialized into the  $|e\rangle$  state, it exponentially decays into the ground state,  $|g\rangle$ . The population in the  $|f\rangle$  state is always close to zero. When the qubit is initialized into the  $|f\rangle$  state, it decays both into the  $|e\rangle$  and  $|g\rangle$  states. However, as time passes the population in the  $|e\rangle$  state also relaxes down to the  $|g\rangle$  state.

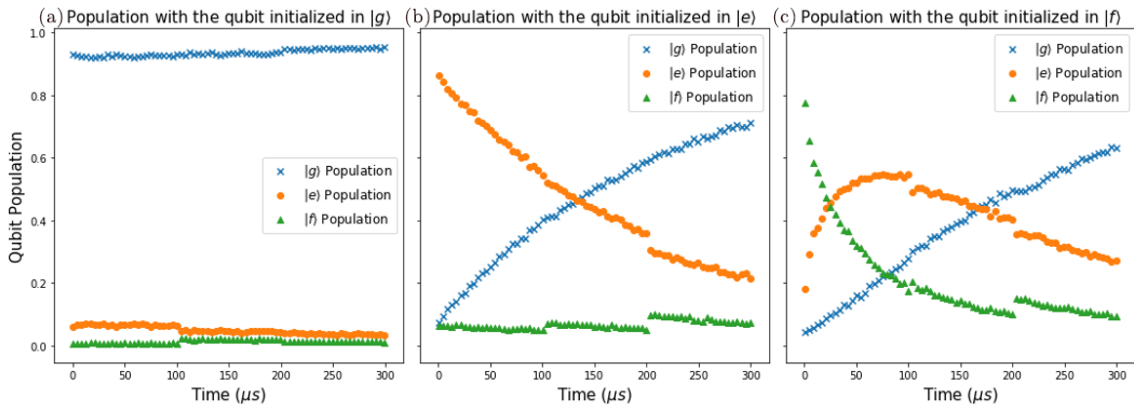


Figure 11: Population of the states initialized in the (a)  $|g\rangle$  (b)  $|e\rangle$ , and (c)  $|f\rangle$  states as a function of time.

### 4.3 Population Dynamics for Various Powers

Figure 12 shows the population dynamics for different amplitudes of the measurement tones. The LDA classifier is retrained for each of the measurement amplitude.

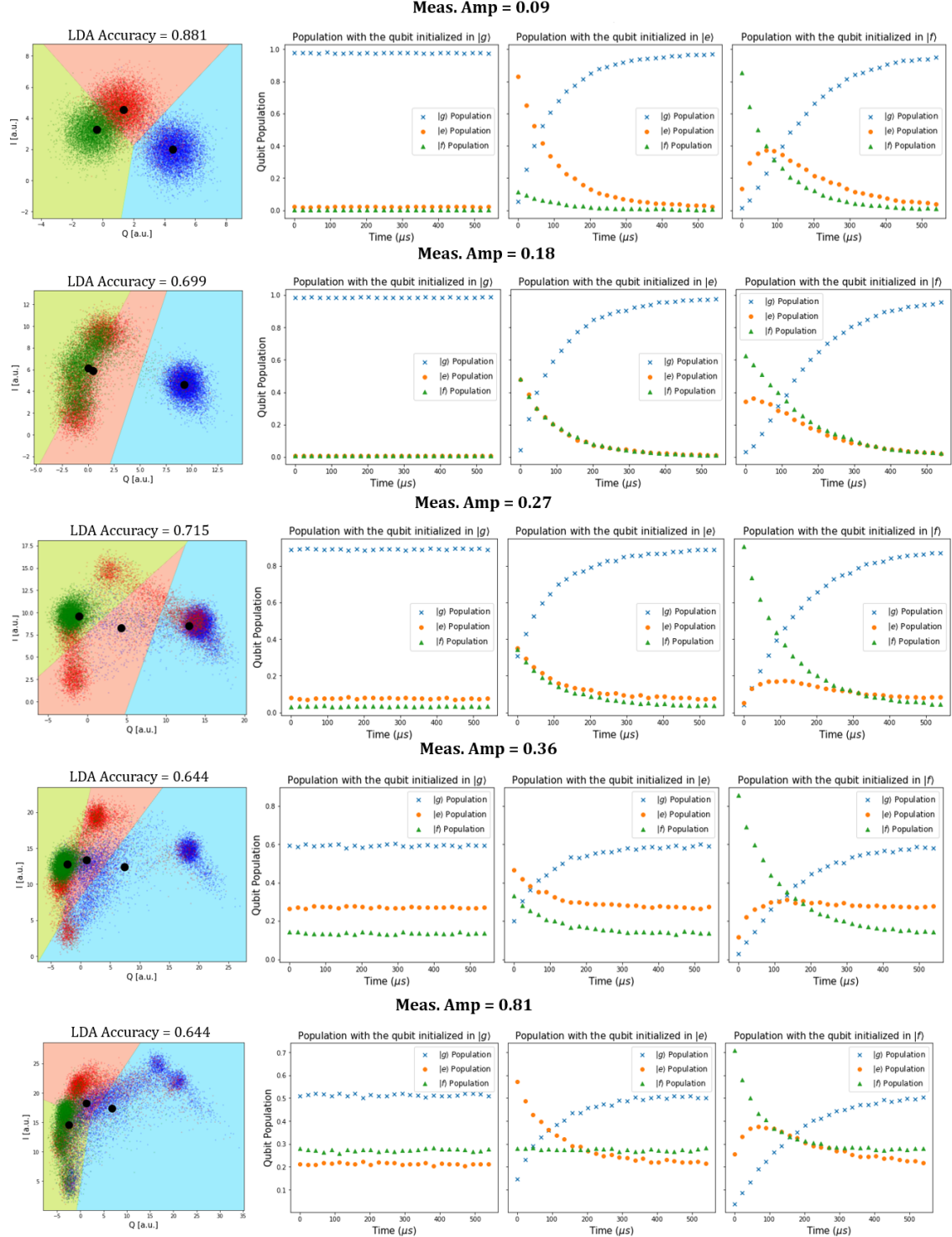


Figure 12: Population dynamics for the measurement amplitude (a) 0.09, (b) 0.18, (c) 0.27, (d) 0.36, and (e) 0.81. The figures on the left show

The curves look smooth, but the initial and steady state populations may be limited by the classifier's accuracy. We see that the LDA accuracy is not too much higher than the coin-flip accuracy, for measurement amplitudes higher than 0.09. This is especially true since the coherent

states corresponding to the excited states are quite distorted.

We tried to debug the “funky” distributions in the IQ plane in two ways

- Waiting initially to ensure that the qubit starts in the ground state.
- Calibrating my own excitation pulses ( $|g\rangle$  to  $|e\rangle$  as well as  $|e\rangle$  to  $|f\rangle$ ), instead of using the ones provided by the backend.

The results from these debugging experiments are shown in Fig. 13. Neither method revealed too much. Waiting initially didn’t change the results too much; the excite state blob is still quite distorted. Using my own pi-pulse highlighted two tails attached to the excited state blob. This is likely because the backend-calibrated pi-pulse includes a DRAG tone, but our pi-pulse doesn’t.

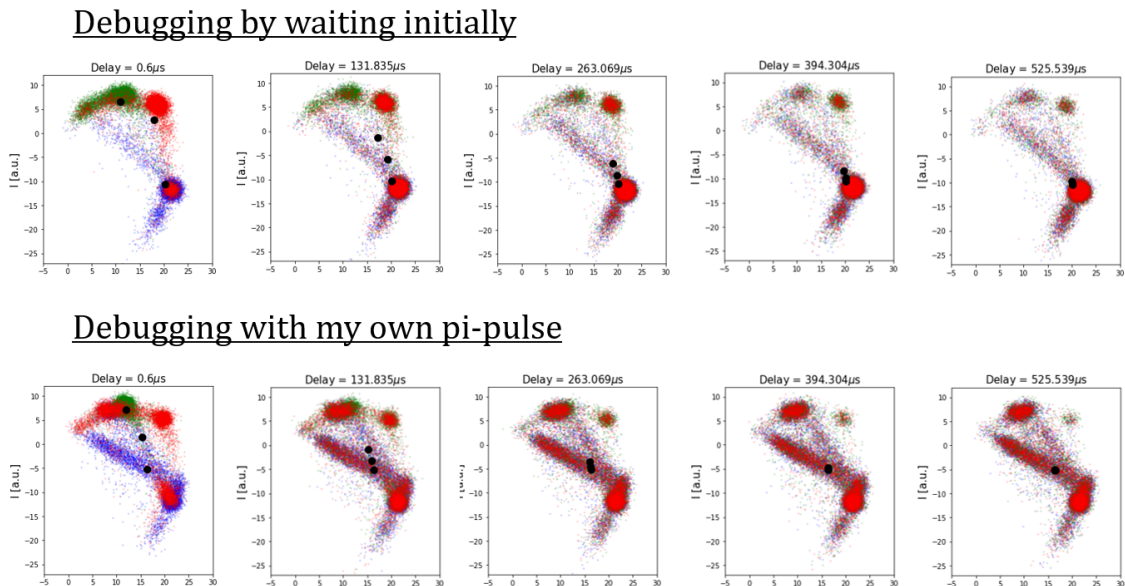


Figure 13: IQ plane as a function of time for two experiments. For the first experiment we wait initially to ensure that the qubit has fully relaxed to the ground state. For the second experiment we use our own pi-pulse, instead of the one calibrated by the backend.

#### 4.4 Abnormalities with the measurement

Qiskit limits users to pack only 75 experiments into a single job, which can often be too limiting. As mentioned before, many of the abnormalities with the measurements were as a result of the way the experiments were packed into jobs. Particularly, the system wasn’t consistent across the boundaries between jobs. Either due to  $T_1$  drift or a change in the way the backend normalized results, we would see fractures in our plots which exactly correspond to these boundaries.

To investigate this further, we packed our experiments in two ways. Method 1 involved packing the ground and excited state experiments, corresponding to a single measurement amplitude into one job. On the other hand, for Method 2 we packed all of the ground state experiment into one job and all the excited state measurements into another. This can be visualized as in 14.

The individual IQ plots can be found in my presentation slides from 2020/06/25. Figures 16 and 15 summarize these results using the means of the collected data.

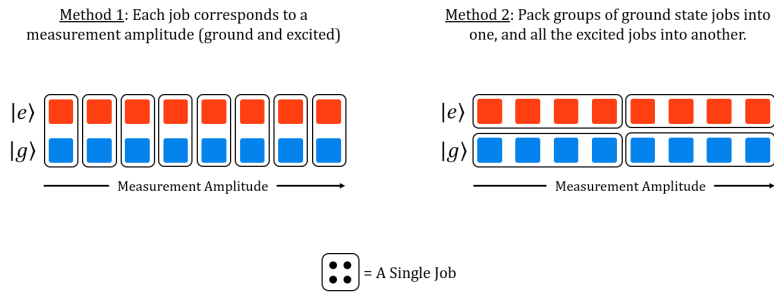


Figure 14: How jobs are packed in (a) Method 1 vs. (b) Method 2.

The pros and cons for each method are as follows:

**Method 1:**

**Pros:**

- Closer to a real measurement
- Great SNR for meas. amps. below 0.662 (ground and excited state responses seem to be sufficiently separated)

**Cons:**

- Takes much longer to run.
- System parameters [e.g.  $T_1$ ] may drift between jobs.
- Non-reproducible effects for higher powers e.g. Excitation into the  $|f\rangle$  state and spuriously exciting the  $|g\rangle$  state to  $|e\rangle$  state.
- Worse linear fit for the diff. between means and vs. meas. amps.

**Method 2:**

**Pros:**

- Runs very quickly. All measurement amplitudes are performed close to each other, so system params are similar.
- Results are always reproducible.
- Backend removes phase difference across meas. amps.
- Better linear fit for the difference between means vs. meas. amp.

**Cons:**

- Might be a phase difference between  $|g\rangle$  and  $|e\rangle$  state measurements; making the SNR seem lower than reality.
- At higher powers, there always seems to be distortion due to the Kerr non-linearity.

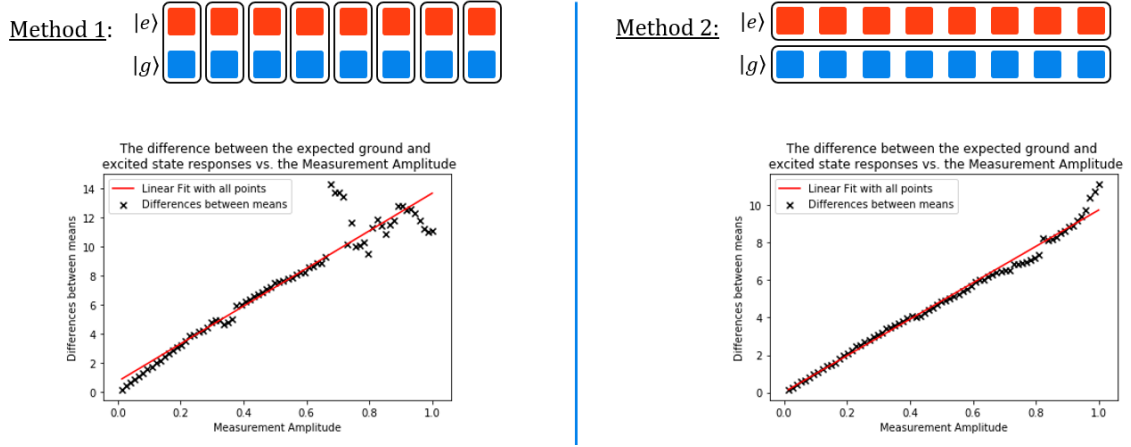


Figure 15: Difference between the ground and excited state means from the single-shot readout IQ measurements. Comparing results from (a) Method 1 and (b) Method 2.

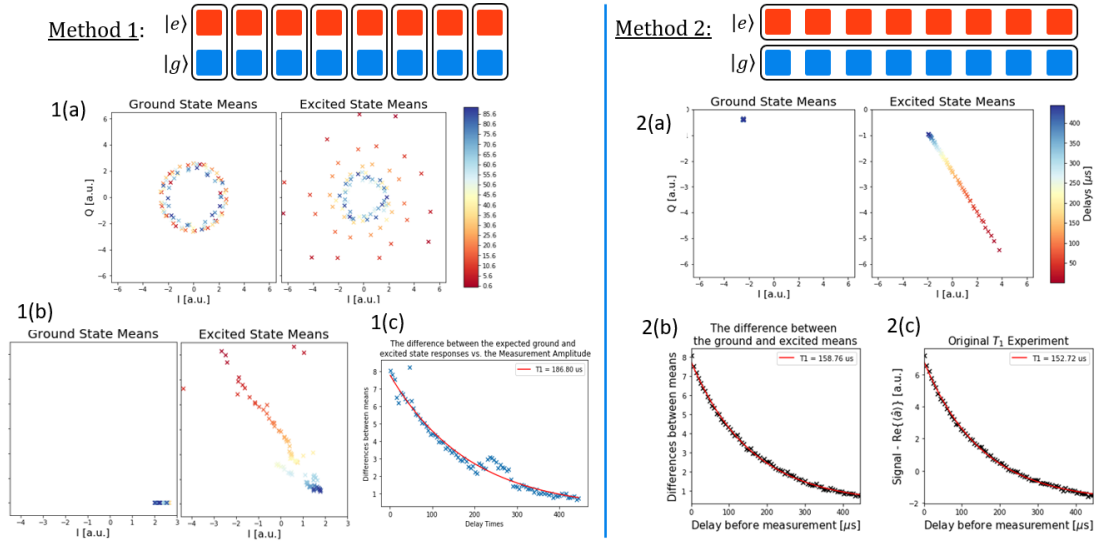


Figure 16: Comparing results from (left) Method 1 and (right) Method 2. The panel (a) on both sides describe the evolution of the mean in the IQ plane. 1(b) shows the time-evolution of the ground and excited state means, but with the frame rotated such that the ground state mean never moves. 1(c) and 2(b) shows the difference between the ground and excited state means as a function of time, with a  $T_1$  exponential fit. 2(c) shows the results from the original  $T_1$  experiment.

## 5 $T_1$ vs Measurement Amplitude

We also sought to investigate the effect of the measurement power on the measured  $T_1$ . I reserved the corresponding systems system, such that the jobs are executed contiguously to limit the effect of  $T_1$  drift. Figures 17 and 18 shows these results from the Valencia and Bogota systems, respectively.

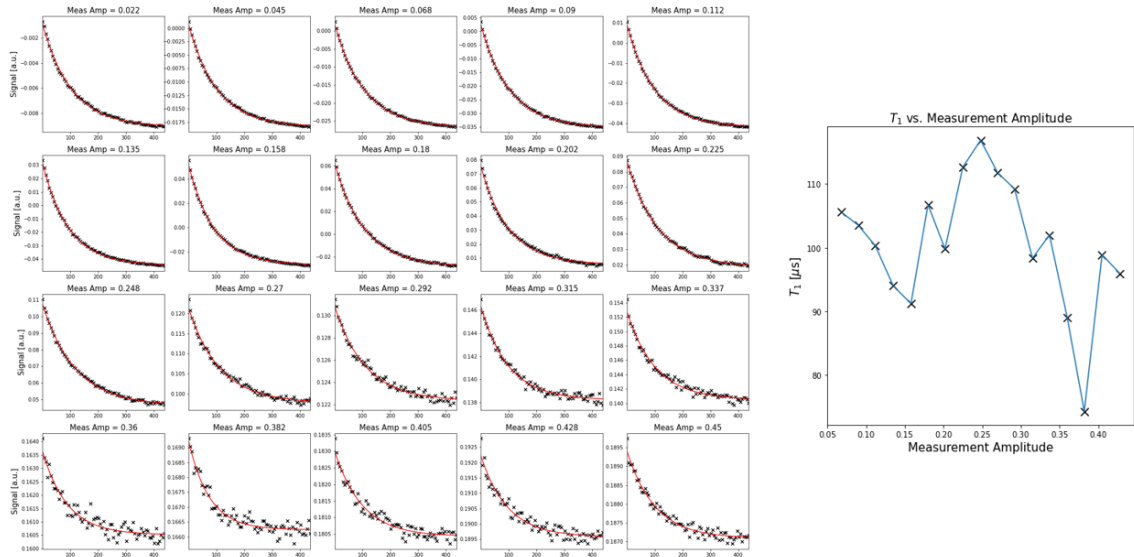


Figure 17:  $T_1$  as a function of the measurement amplitude (on Valencia). The individual exponential fits are shown on the left.

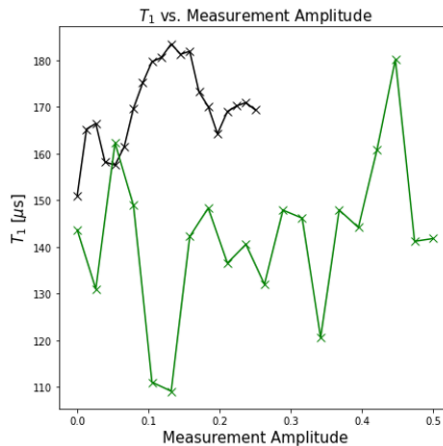


Figure 18:  $T_1$  as a function of the measurement amplitude (on Bogota). The blue and black traces represent results from the same experiment run on different days and spanning a different range of measurement amplitudes. The black trace was a finer one between 0 and 0.25, whereas the blue one was a wider one between 0 and 0.5. The backend calibrated measurement pulse for this device had an amplitude of 0.1.

Observe from Fig. 17, that as we increase the measurement power the decay plot become more noisy. However, neither Fig. 17 nor Fig. 18 shows any promising trend between  $T_1$  and the measurement power. Particularly, Fig. 18 shows that the  $T_1$  measured for the same power on different days resulted in vastly different results.

We believe that there may be two factors at play. Firstly, the  $T_1$  drift intrinsic to the respective devices may result in error-bars so large that they mask any trend caused by varying the measurement power. We were informed by Abe Asfaw at IBM that the  $T_1$  drifts by 15%, per day, from morning to evening. Secondly, we think that the powers Qiskit permits us to use are actually quite

low. This was substantiated by Abe Asfaw.

## 6 Discussion on the Limitations of Open-Pulse and Unsuccessful Experiments

Very candidly, performing experiments on Qiskit Open-Pulse was a very tall order. The system was clearly in its naissance stages, and we frequently ran into road-blocks while trying to stretch what was possible. When we began our collaboration with the HouckLab, on the same project, I was pleasantly suprised as to how quickly they were able to collect data.

Here is a summary of the difficulties I had with the Qiskit Open-Pulse system (as of August 2020):

- The IBM researchers were unwilling to disclose how the dimensionless measurement amplitude parameter translated to units of voltage or power (in dB).
- We're only allowed to use measurement amplitudes at low powers. As such, we weren't able to fully investigate the effects of increasing the amplitude of the measurement tone on the measured  $T_1$ .
- The measurement (integration) time is truncated by Qiskit. As such, we were unable to take the long measurements required by the cavity sweep experiment and unable to derive  $\chi$  for most of systems.
- Qiskit only allows the users to pack 75 experiments per schedule. This is often very limiting, especially when investigating how all the three states:  $|g\rangle$ ,  $|e\rangle$ , and  $|f\rangle$ , vary with a parameter.
- Because 75 experiments are often too few, job packaging matters a lot. Particularly, since qiskit performs phase correction between different schedules within the same job. The IBM researchers were unwilling to disclose their phase correction and backend data processing algorithms.
- The limited memory capacity of Qiskit jobs was very restricting. As a result, we weren't able to perform more sophisticated measurements such as two-tone spectroscopy or filling the cavity before measurement. When trying out these experiments, we would receive an error claiming that the number of points in our schedule exceeds the limit.
- Since the qubits are a shared resource, we aren't aware about the experiments the most recent experiments that our qubits have been through. As such, we can never guarantee the initial state of our qubit. This is a very likely reason of the irreproducibility and inconsistencies across jobs and measurements taken on different days.
- Qiskit doesn't allow the user to perform any experiments after measuring the qubit. As such, we weren't able to implement post-selection in our experiments. This would have allowed us to verify that we start off in the ground state, rather than an arbitrary mixed state. We believe that having confidence in our starting state, we would've been able to avoid distorted coherent states corresponding to the excited states.
- Time evolution of the cavity coherent states contained very valuable information for comparison with theory. However, the raw data (which would be accessible through measurement-level 0 in qiskit) isn't yet implemented. We figured out a work-around to this, by introducing a delay between the time we start pumping the cavity and when we begin to integrate the measured field. However, we were only able to acquire the dynamics up to  $3\mu s$ , which is incredibly small in comparison to the time-scale of the qubit lifetimes. For delays greater than  $3\mu s$ , we rapidly ran into memory errors.
- The experiments on the IBMQ devices are incredibly slow to work with. It took a tenth of the time to perform most of the  $T_1$  vs. Measurement amplitude experiments with the HouckLab qubits. I mean the absolute time to execute the experiments, not including any time writing code and setting up the experiment.

I do not blame IBM for the Qiskit's shortcomings, as mentioned above. The service is hardly a year old, and I'm looking forward to seeing it develop into a ubiquitous research resource. However, as it currently stands, the service is far too underdeveloped to be used for hardware-level research.